

Density-functional theory guided advances in phase-change materials and memories

Wei Zhang, Volker L. Deringer, Richard Dronskowski, Riccardo Mazzarello, Evan Ma, and Matthias Wuttig

Phase-change materials (PCMs) are promising candidates for novel data-storage and memory applications. They encode digital information by exploiting the optical and electronic contrast between amorphous and crystalline states. Rapid and reversible switching between the two states can be induced by voltage or laser pulses. Here, we review how density-functional theory (DFT) is advancing our understanding of PCMs. We describe key DFT insights into structural, electronic, and bonding properties of PCMs and into technologically relevant processes such as fast crystallization and relaxation of the amorphous state. We also comment on the leading role played by predictive DFT simulations in new potential applications of PCMs, including topological properties, switching between different topological states, and magnetic properties of doped PCMs. Such DFT-based approaches are also projected to be powerful in guiding advances in other materials-science fields.

Introduction

The global demand for data storage is growing ever faster in the present “information age.” Silicon-based flash memories, which have dominated the nonvolatile storage market so far, seem to have reached their performance and scalability limits, and massive efforts are underway to develop new memory materials. Among these, phase-change random-access memory (PRAM) based on phase-change materials (PCMs) shows great promise.^{1–4} If superior PCMs materials could be identified, a universal device⁵ could be realized that could potentially replace magnetic hard drives, flash memories, and dynamic random-access memory.

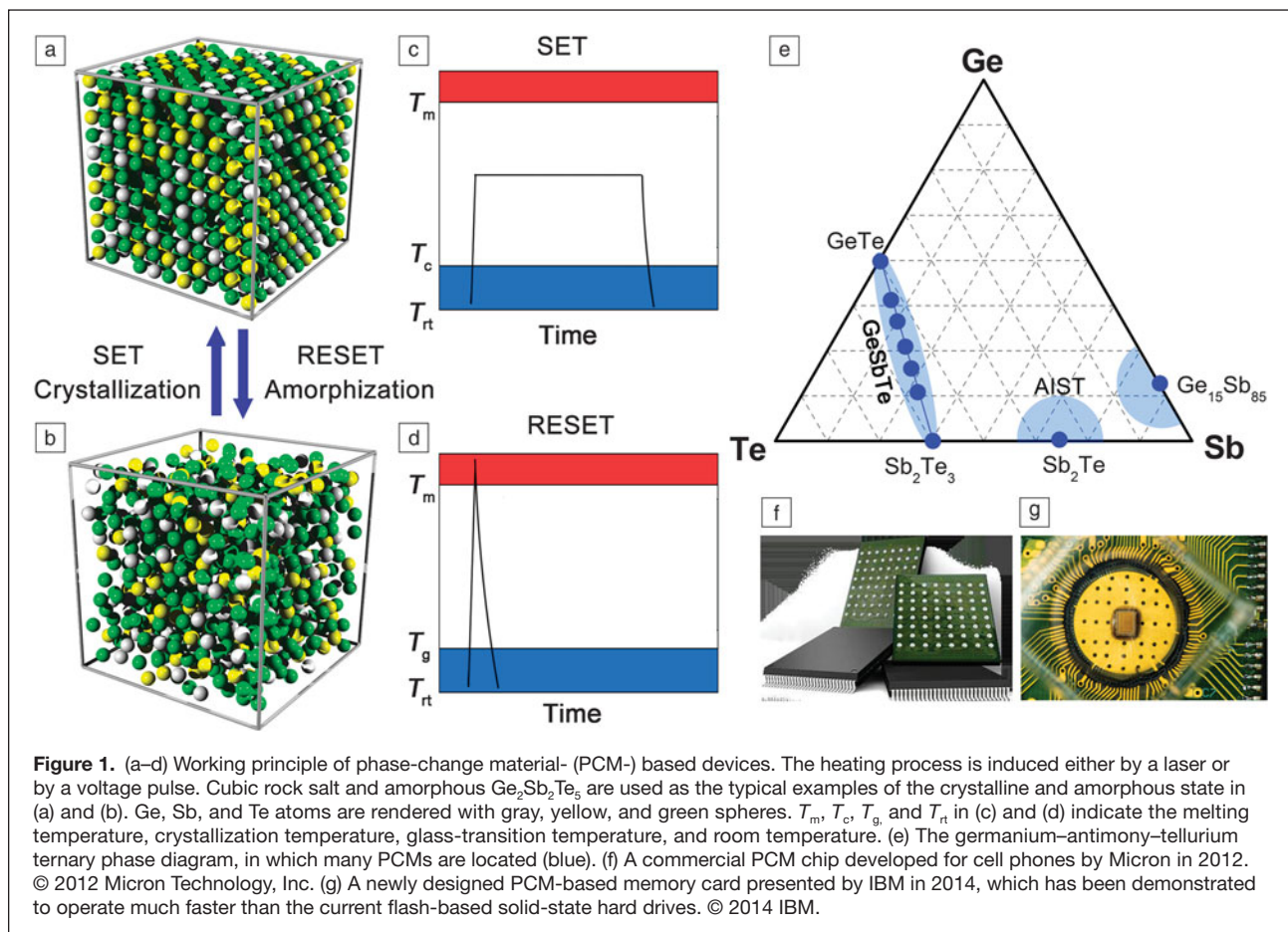
The storage concept of PCMs is sketched in **Figure 1**. At room temperature, these materials have at least two metastable phases, amorphous and crystalline, with pronounced contrast in optical reflectivity and electrical resistance; this represents the two logic states “0” (amorphous) and “1” (crystalline). Upon application of a long, medium-intensity voltage or laser pulse, the amorphous region is locally annealed and crystallized (“SET”). Using a short, high-intensity voltage or laser pulse, the focused region is instead heated above its melting

temperature; subsequent rapid cooling yields a disordered amorphous mark (“RESET”). To read out information, a small current pulse or laser beam is used that does not alter the state of the bit.^{1,3}

The most successful candidates for phase-change technology have been identified in the ternary germanium–antimony–tellurium system^{1,3} (Figure 1e). There are three main families: tellurides along the quasibinary GeTe–Sb₂Te₃ tie line (denoted as GST in the following); alloyed or, in the community’s jargon, “doped” Sb₂Te (prominently, silver–indium–antimony–tellurium [Ag–In–Sb–Te; AIST] alloys); and derivatives of elemental antimony such as Ge₁₅Sb₈₅. Some emerging electronic data-storage and memory products that employ PCMs are shown in Figure 1f (a commercial PCM chip developed for cell phones) and Figure 1g (a PCM-based memory card).

Computer simulation plays a key role in modern materials science. Simulations have been supplementing experiments for many years and are now revealing truly predictive power. Density-functional-based electronic-structure theory⁶ (DFT) and molecular dynamics⁷ (DFMD) simulations can predict characteristics of “real” materials with quantum-mechanical

Wei Zhang, Xi'an Jiaotong University, Xi'an, China; wzhang0@mail.xjtu.edu.cn
Volker L. Deringer, RWTH Aachen University, Aachen, Germany; volker.deringer@ac.rwth-aachen.de
Richard Dronskowski, RWTH Aachen University, Aachen, Germany; drons@HAL9000.ac.rwth-aachen.de
Riccardo Mazzarello, RWTH Aachen University, Aachen, Germany; mazzarello@physik.rwth-aachen.de
Evan Ma, Johns Hopkins University, USA; ema@jhu.edu
Matthias Wuttig, RWTH Aachen University, Aachen, Germany; wuttig@physik.rwth-aachen.de
DOI: 10.1557/mrs.2015.227



accuracy. Thanks to the exponential growth of supercomputing power, state-of-the-art simulations can now access the time and length scales of the physical processes in phase-change memory cells.

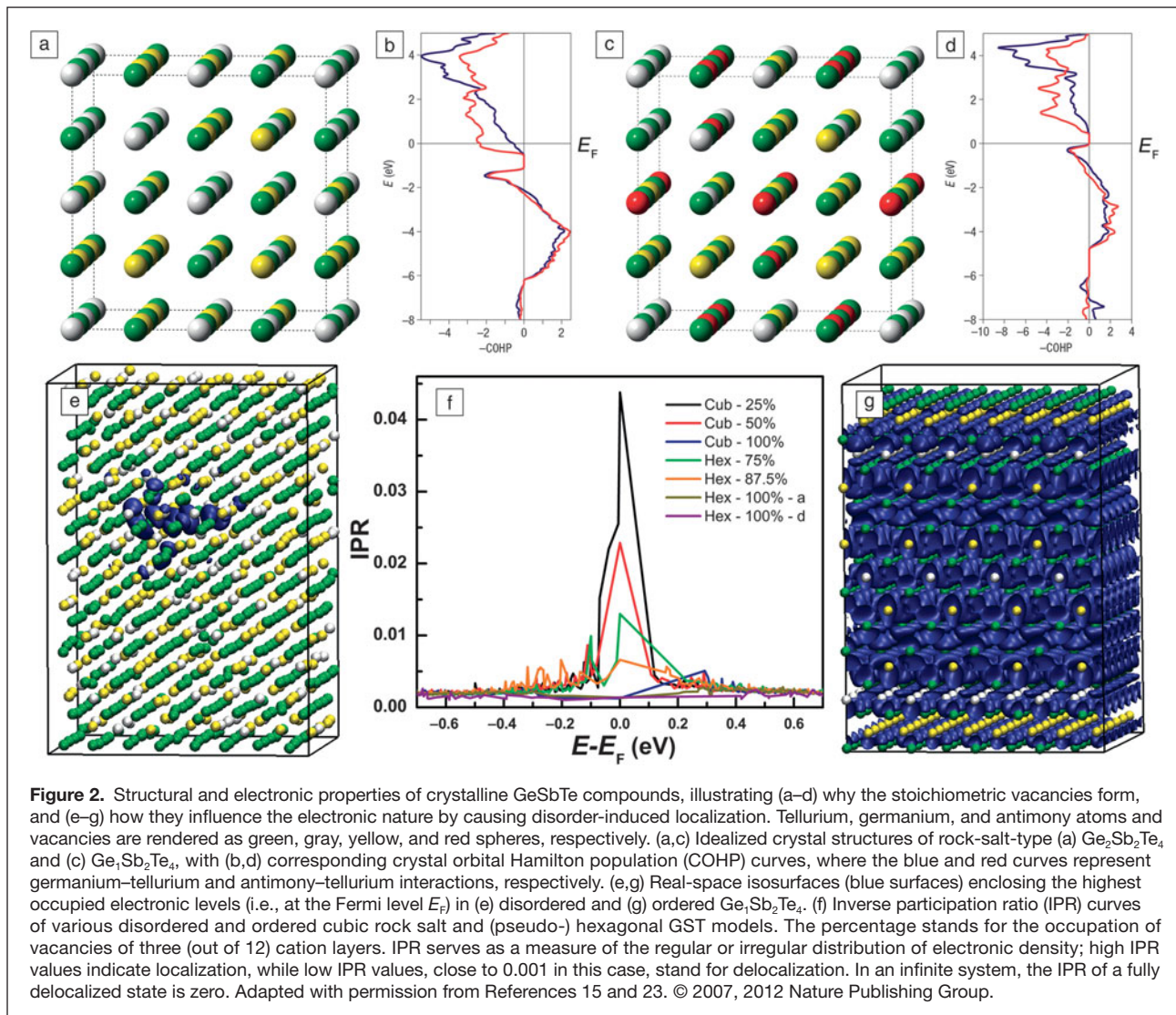
In this overview article, we summarize DFT-guided advances in the materials science of PCMs and in PRAM technology. The article is structured as a list of questions that, in our opinion, address several crucial issues regarding PCMs. Some of the questions have been resolved, and some are still being pursued. Answering them will also inspire important advances beyond the field of PCMs.

What makes crystalline and amorphous PCMs so different?

The first and quick answer is “structure.” Although atomic structure is very important, there is even more. The different properties of the two phases are caused by very complex aspects on the atomic scale that have recently been reviewed.⁸ Even though current research is focusing on electronic memories, the most important consumer products based on PCMs so far have been optical discs (e.g., rewriteable Blu-ray discs); naturally, many studies have been devoted to the optical property contrast of PCMs. Based on experiments⁹ and later corroborated by theory,^{10,11} it was suggested that crystalline PCMs are

characterized by a generic bonding mechanism, namely, resonance bonding, that originates from the resonance between different bonding configurations. This mechanism leads to electron delocalization and high dielectric constants. The misalignment of directional p bonds weakens resonance bonding and, thus, lowers the dielectric constant and changes the optical matrix elements significantly.¹¹ As angular disorder in p -bonding prevails in amorphous PCMs,¹² the origin of the optical contrast is thus identified. It is such microscopic understanding that paves the way to discover new PCMs with optimal properties.¹⁰

Metastable GST alloys form rock-salt-type structures upon fast crystallization, with a fully occupied tellurium sublattice and an interpenetrating one in which germanium, antimony, and vacancies are randomly arranged.^{13,14} Why is this stoichiometric amount of vacancies formed in the first place? This question was addressed using DFT¹⁵—first, computing energies and then dissecting the electronic structures with the help of a quantum-chemical bonding indicator, dubbed crystal orbital Hamilton population (COHP)¹⁶ analysis. Starting from a hypothetical rock-salt $\text{Ge}_2\text{Sb}_2\text{Te}_4$ alloy, germanium atoms were gradually removed from the model structure, until the experimentally observed composition of $\text{Ge}_1\text{Sb}_2\text{Te}_4$ was reached (**Figure 2a** and 2c). Large negative formation energies were



found, suggesting that the presence of vacancies is favorable, but a full understanding came from bonding theory (Figure 2b and 2d). The hypothetical, fully occupied lattice of $\text{Ge}_2\text{Sb}_2\text{Te}_4$ exhibits significant antibonding interactions ($-\text{COHP} < 0$) at the Fermi level E_F that decrease when germanium atoms are removed; this is because the cationic atoms donate electrons to the host structure. Nonetheless, a certain amount of occupied, antibonding levels remains in $\text{Ge}_1\text{Sb}_2\text{Te}_4$, and similar observations were made for the binary parent compounds GeTe^{17} and Sb_2Te_3 .¹⁸

What causes the electronic contrast?

Both amorphous and cubic GST are semiconducting, with bandgaps of 0.5–1.0 eV. Nevertheless, at room temperature, the electrical resistance values of the two metastable phases differ by more than three orders of magnitude.¹⁹ This contrast stems from the interplay between disorder strength and carrier concentration. In the amorphous state, E_F is pinned in the middle of the bandgap as a result of disorder, and the carrier

concentration is low. Rock-salt GST and related materials, on the other hand, exhibit so-called self-doping and *p*-type conductivity. DFT-based studies^{20,21} traced this behavior back to the presence of excess vacancies on germanium/antimony sites (i.e., beyond those stoichiometric vacancies shown in Figure 2c). Consequently, E_F is shifted to the valence band, and large concentrations of hole carriers arise.¹⁹

Interestingly, upon further thermal annealing of crystalline GST, the electrical resistance decreases by another three orders of magnitude at room temperature.¹⁹ Low-temperature transport measurements also revealed exciting phenomena: namely, disorder-induced electron localization and metal–insulator transitions.^{19,22} Zhang et al. elucidated the microscopic origins of these phenomena through large-scale DFT simulations.²³ Rock-salt-type and pseudohexagonal structural models of GST containing up to 3584 atoms were subjected to DFT analysis. Anderson (disorder-induced) localization of electron wave functions was observed in the disordered models (Figure 2f): Through computations of the atomic projections

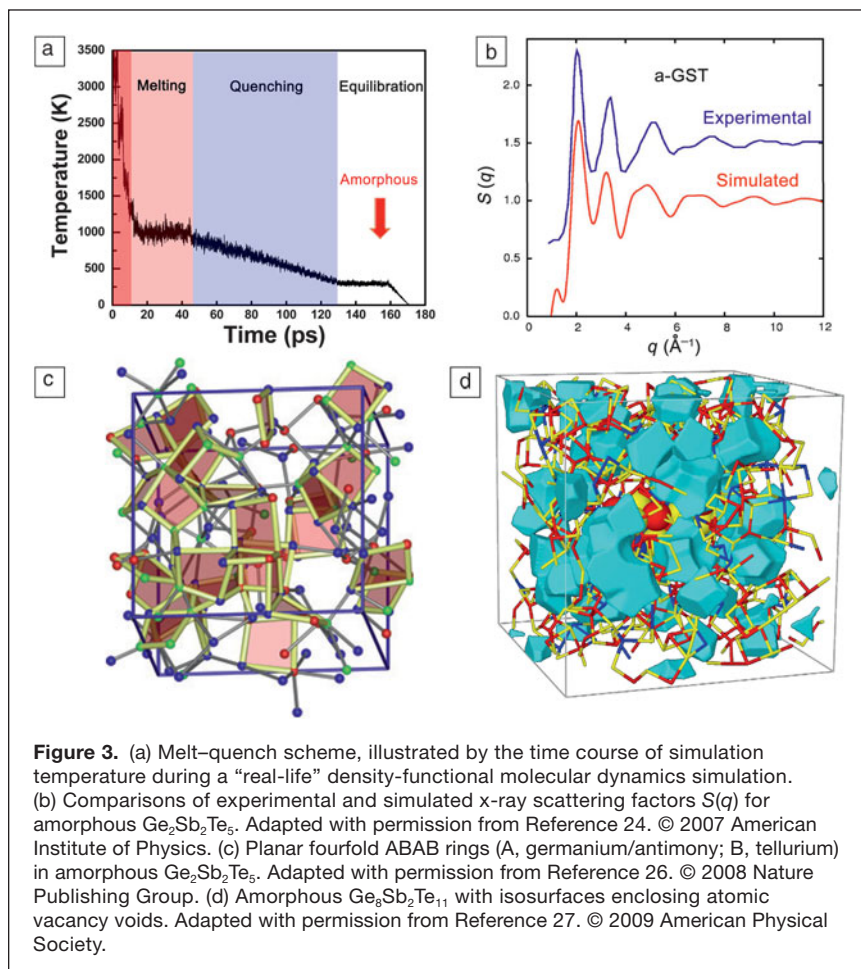
of the electronic density of states, the inverse participation ratio (a parameter that characterizes the degree of localization of a wave function), and the spatial distribution of electronic wave functions, it was shown that the states near E_F are exponentially localized inside vacancy-rich regions. The simulations also indicated that vacancy clusters (not voids) become ordered into vacancy planes upon progressive thermal annealing, driving the structural transition from cubic to layered structures and, independently, leading to extended electronic states and metallic behavior in $\text{Ge}_1\text{Sb}_2\text{Te}_4$ (Figure 2e and 2g).

How does one simulate an amorphous material?

Given that crystalline PCMs are already complex, the same is even more so for their amorphous (glassy) counterparts. The first DFMD simulations of amorphous PCMs were reported independently by Caravati et al.²⁴ and Akola and Jones²⁵ in 2007. Amorphous (a-) $\text{Ge}_2\text{Sb}_2\text{Te}_5$, as well as a- $\text{Ge}_2\text{Sb}_2\text{Te}_5$ and a-GeTe, respectively, were produced by a melt-quench scheme, in which a simulation cell is loaded with atoms, randomized at very high temperature, and then rapidly cooled to achieve an amorphous structure (Figure 3a). The x-ray scattering factor $S(q)$ was calculated based on the trajectory of a- $\text{Ge}_2\text{Sb}_2\text{Te}_5$ at room temperature and compared to experiments²⁴ (Figure 3b). Clearly, the overall shape and primary peak positions of $S(q)$

were well-recovered by the calculations. DFMD simulations also allow for the determination of quantities that are not easily accessible experimentally. The analysis of primitive rings, a typical indicator for medium-range order, revealed that fourfold rings dominate over the others and that most rings are planar with ABAB patterns (A, germanium/antimony; B, tellurium)^{24–26} (Figure 3c). In addition, vacancy voids are abundant in amorphous PCMs^{25,27,28} (Figure 3d). Both observations were suggested to be linked to the materials' ability to crystallize rapidly.

Local structural motifs in amorphous PCMs have been under very active study since a seminal work by Kolobov et al.²⁹ in 2004. On the basis of extended x-ray absorption fine-structure spectroscopy (EXAFS) and x-ray absorption near-edge structure spectra of amorphous and recrystallized GST, the authors proposed an umbrella-flip model in which germanium atoms switch back and forth between octahedral and interstitial tetrahedral sites. This model provided an intuitive picture of the phase transitions; nevertheless, the real processes turned out to be far more complex from recent experiments and simulations (as discussed in the next section). In DFMD simulations of melt-quenched a-GST,^{24,25} only roughly one-third of germanium atoms were found in tetrahedral environments (denoted Ge^T), whereas the residual germanium atoms were found in defective octahedral configurations (Ge^O ; Figure 4a),



as were all antimony and tellurium atoms. Coordination numbers and nearest-neighbor bond lengths were extracted independently from EXAFS measurements and DFMD simulations: The results agreed fairly well, except that the simulated germanium–tellurium bond length was about 6% larger than the experimental value. Unfortunately, an ultimate verdict based on either EXAFS (which involves indirect observations) or DFT (which might have intrinsic shortcomings) is very difficult, especially when it comes to small structural variations. In particular, the aforementioned bond-length deviation, the existence of Ge^T , and the nature of bonding have been under debate for more than a decade.^{30–39}

Indeed, the observation of Ge^T in a-GeTe and a-GST is puzzling, as such a motif cannot be found in any crystalline (i.e., stable) form of the compounds: Exclusively octahedral-like coordination prevails. Furthermore, most Ge^T atoms in the amorphous phase are predicted to form at least one homopolar germanium–germanium bond,²⁴ again, at variance with the crystalline phases. In a 2014 report, a new theoretical chemical approach was employed to study the local nature of these different structural fragments.⁴⁰ This tool is conceptually similar to previous COHP analyses (Figure 2), but different in detail, in that it extracts the local chemical information from numerically

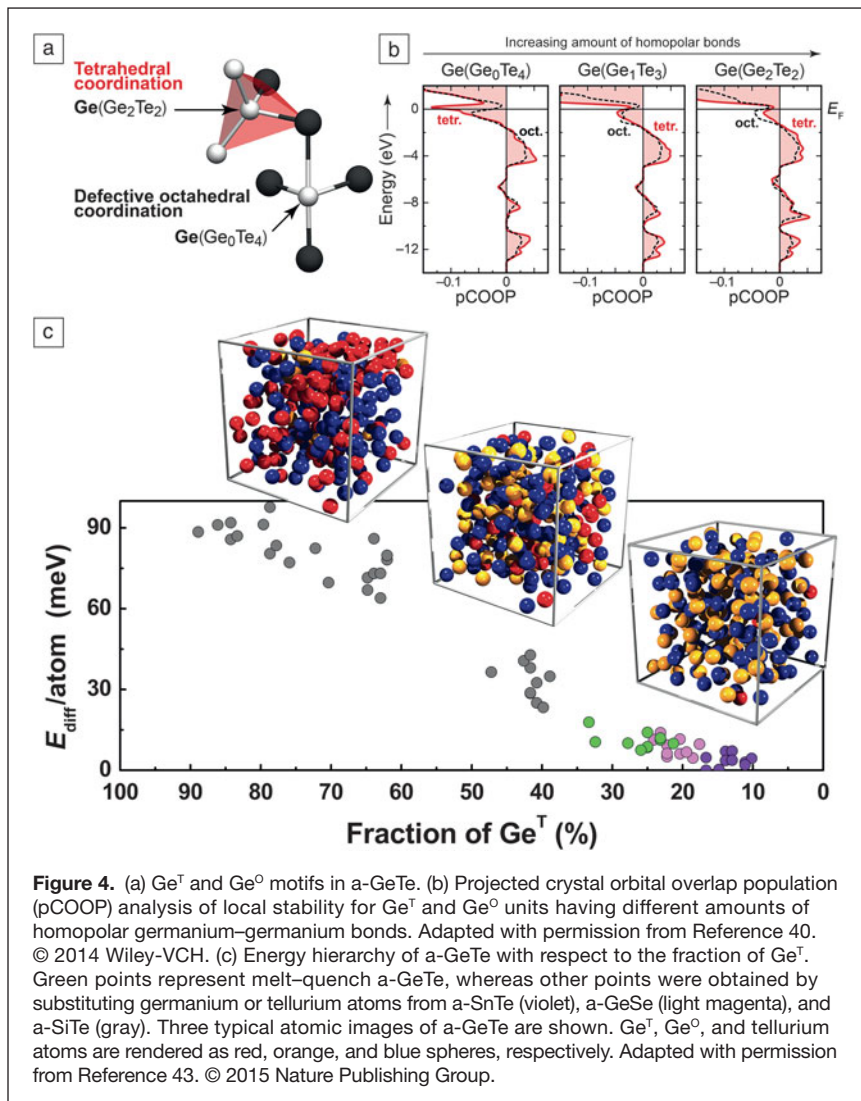


Figure 4. (a) Ge^{T} and Ge^{O} motifs in a-GeTe. (b) Projected crystal orbital overlap population (pCOOP) analysis of local stability for Ge^{T} and Ge^{O} units having different amounts of homopolar germanium–germanium bonds. Adapted with permission from Reference 40. © 2014 Wiley-VCH. (c) Energy hierarchy of a-GeTe with respect to the fraction of Ge^{T} . Green points represent melt–quench a-GeTe, whereas other points were obtained by substituting germanium or tellurium atoms from a-SnTe (violet), a-GeSe (light magenta), and a-SiTe (gray). Three typical atomic images of a-GeTe are shown. Ge^{T} , Ge^{O} , and tellurium atoms are rendered as red, orange, and blue spheres, respectively. Adapted with permission from Reference 43. © 2015 Nature Publishing Group.

efficient plane-wave basis sets,^{41,42} which are routinely used in DFMD simulations of PCMs and other amorphous materials. As a result, the importance of homopolar bonds in stabilizing Ge^{T} fragments could be addressed and quantified. Figure 4b compares projected crystal orbital overlap populations for various Ge^{T} and Ge^{O} units in a-GeTe. Obviously, Ge^{T} units exhibit antibonding interactions at E_F , but these interactions drop significantly with the onset of homopolar germanium–germanium bonding, whereas there is no pronounced change in the bonding nature of Ge^{O} . Because the heat of formation of GeTe is small, homopolar bonds are present in the molten state, and upon subnanosecond quenching, these bonds are frozen in and give rise to a fraction of Ge^{T} units.⁴³ Hence, Ge^{T} is ultimately transient in nature, as discussed further in the text.

Resistance drift (i.e., an increase in resistance over time) in amorphous PCMs^{44,45} is an outstanding problem for both fundamental research and memory technology, as it hinders multilevel storage applications. Because this drift occurs on time scales of seconds, minutes, or days, it is inaccessible to

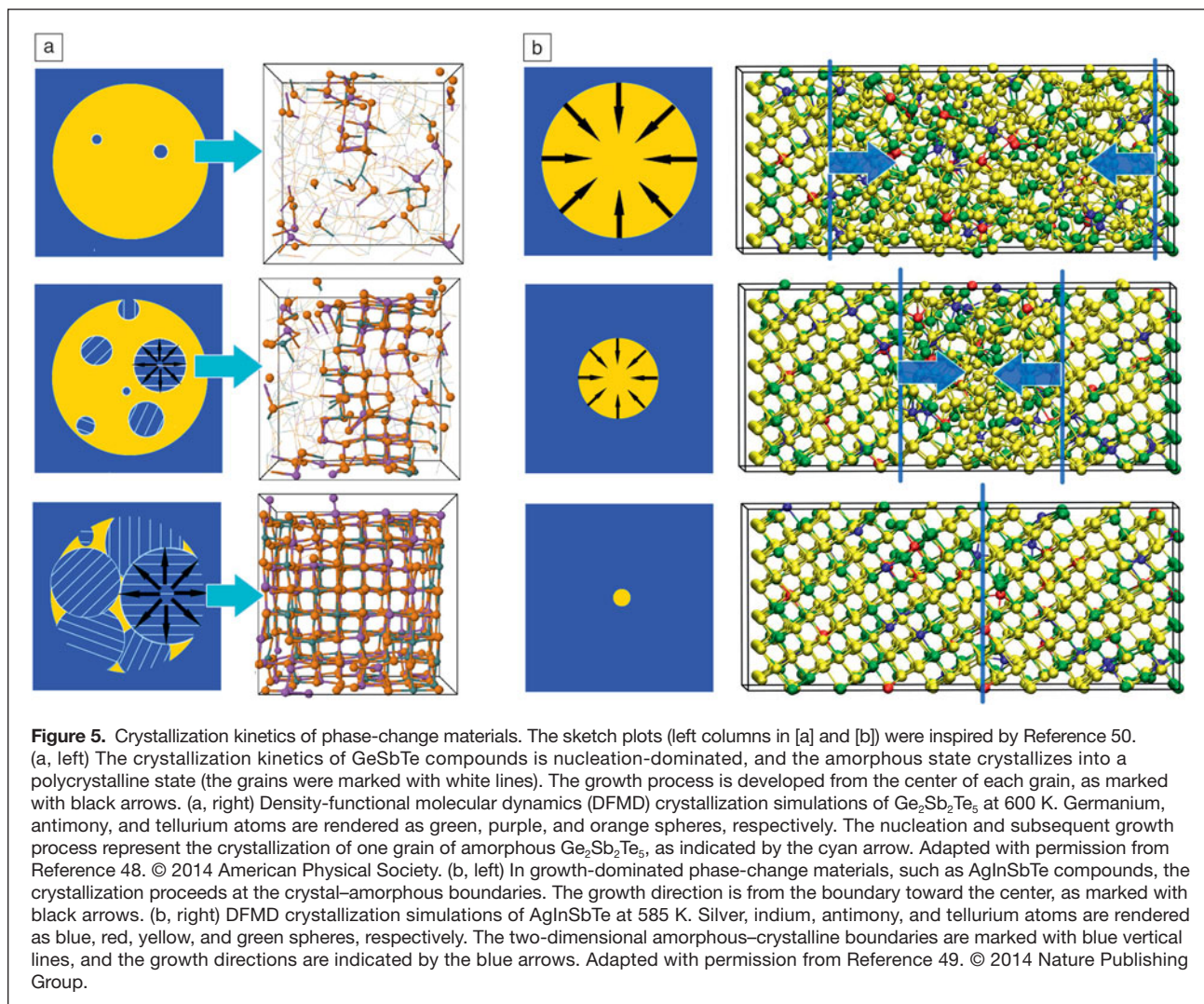
crystallization process at high temperature can be directly simulated.

Two different crystallization stages have been identified in PCMs,⁵⁰ namely, nucleation and growth, as sketched in **Figure 5**. In 2008, Hegedüs and Elliott²⁶ achieved the first DFMD crystallization simulation of a nucleation-dominated PCM, $\text{Ge}_2\text{Sb}_2\text{Te}_5$, using system sizes of 63–90 atoms. Later, the same group⁵¹ crystallized a larger 180-atom model, which enabled a reasonable estimate of the critical nucleus size (24–44 atoms) and growth rate (~ 5 m/s). The fast crystallization was attributed to the high density of planar fourfold ABAB rings. This point was partly challenged by Kalikka and co-workers,^{48,52} who reported that the ABAB squares can break and re-form during crystallization as a result of the diffusive nature of the germanium, antimony, and tellurium motions at high temperatures and that this high atomic mobility is a prerequisite for fast growth. Their simulations comprised 460–648 atoms, and representative snapshots of the crystallization trajectory are shown in Figure 5a.

“brute-force” DFMD simulations. Nonetheless, other approaches are possible, and recently, Raty et al.⁴³ were able to identify the microscopic origin of the resistance drift in a-GeTe, based on DFT simulations. Employing the chemical substitution method,^{33,37} the authors generated structural models of a-GeTe, in which the fraction of Ge^{T} ranged from 10–90% (Figure 4c). The models with the lowest amount of Ge^{T} yielded the lowest energy (violet points); importantly, they were more stable than “standard” melt-quenched a-GeTe models (green points). Thus, a-GeTe should evolve toward a network with less Ge^{T} . This lowers the energy and stress of the system, and it removes localized midgap electronic states. It was also shown that, concomitantly, the Peierls distortion (a local distortion towards more asymmetric environments, consisting of short and long bonds, which lowers the total energy) gets more pronounced in the aged amorphous network.⁴³ As a result, the optical bandgap rises, and, thus, so does the resistance, whereas the dielectric constant is lowered.^{46,47}

What can DFT tell us about switching kinetics—and what can it not tell us?

The crystallization speed of PCMs spans over 17 orders of magnitude: At room temperature, the amorphous phases are metastable for decades, whereas at elevated temperatures (600–700 K), they crystallize within nanoseconds. This property is critical for data storage. Current supercomputers have made DFMD simulations of $\sim 1,000$ -atom models feasible, with runs over nanoseconds,^{48,49} in other words, the



In early 2015, Ronneberger et al.⁵³ employed metadynamics,⁵⁴ an enhanced sampling technique, to accelerate the formation of critical nuclei. Within a 460-atom supercell, quasi-spherical crystal clusters of ≤ 100 atoms were found to be stable. Crystal growth at the interface was studied as well, and the estimated growth speed of ~ 1 m/s agreed reasonably with recent experiments.^{55–57} All of these simulations have shown that the pronounced disorder in metastable rock-salt GST is a consequence of fast crystallization. The atoms near the crystal surface have very limited time to arrange themselves to impinge on the crystalline interface, so a highly disordered structure results. Based on DFT total-energy calculations, Sun et al.⁵⁸ and Da Silva et al.⁵⁹ proposed an ordered rock-salt GST with regular atomic and vacancy layers. Given sufficient time to guarantee a smooth crystal-growth process, such a phase could also be produced, for example, by using molecular beam epitaxy techniques.⁶⁰

Another study showed that the crystallization time limit of GST can be further reduced by applying a constant low voltage during the crystallization process.⁶¹ DFMD simulations

indicated that this reduction stems from structural preordering induced by voltage.⁶¹ To further increase the accessible system size, Sosso et al.⁶² developed a DFT-trained neural-network potential obtained by fitting the GeTe hypersurface that afforded new atomistic insight into the atomic-scale processes during crystallization of this compound.^{63,64}

As mentioned in the introduction, a silver-/indium-substituted Sb_2Te alloy (AIST) is a powerful material for data storage. In contrast to the nucleation process in GST, the dominant crystallization mechanism in AIST is growth from the amorphous–crystalline interface (Figure 5b). In 2014, Zhang et al. performed DFMD simulations of AIST crystallization, using up to 810-atom systems.⁴⁹ Because AIST crystallizes in the stacked layer structure,⁶⁵ two adjacent crystalline layers along [0001] were fixed during the melt–quench run, creating two amorphous–crystalline boundaries. Upon heating at 585 K, the system quickly crystallized, and smooth growth along the boundary was observed (Figure 5b); the thus-obtained growth rate and recrystallized structure agreed with recent experiments.^{65,66} The fast growth was explained by the high atomic

mobility near the very thin interface, together with a very effective sticking process.⁴⁹

Despite these successes, DFMD simulations encounter a serious problem at lower temperatures in the range of 450–500 K, where the obtained growth speeds are orders of magnitude larger than experimental values.⁴⁹ This problem is attributed to the ultrahigh fragility of AIST⁶⁶ and the too-high quenching rates employed in DFMD simulations, which are typically 100–1000 times higher than experimental rates (because of the very high computational costs). The potential energy landscape of fragile systems is very complex,⁶⁷ and high quenching rates lead to insufficient exploration of phase space.⁴⁹ Therefore, at low temperatures, the simulated crystal growth is much faster than in reality.⁶⁶

As such, simulating the crystallization dynamics at lower temperatures still remains an open question. An understanding of fragility is crucial for phase-change data storage: High fragility guarantees a dramatic change in the temperature dependence of the growth velocity, which makes the crystallization process ultrafast at high temperature, but extremely slow at room temperature.^{49,56,57,66}

What challenges and opportunities lie ahead?

DFT has made a major difference in our current understanding of PCMs. In the following, we briefly outline a few other examples where DFT is being attempted as we speak and where DFT for PCM is heading in the near term. The structural parent compound Sb_2Te_3 is among the best-known topological insulators (TIs),^{68,69} which represent a new class of electronic materials with an insulating bulk state and a topologically protected conducting surface state (due to time-reversal symmetry and strong spin-orbit coupling).⁶⁹ Interestingly, layered $\text{Ge}_2\text{Sb}_2\text{Te}_5$ with the Petrov sequence, $-\text{Te}-\text{Sb}-\text{Te}-\text{Ge}-\text{Te}-\text{Te}-\text{Ge}-\text{Te}-\text{Sb}-(\text{Te}-)$ (the bracket indicates the periodic image), has been predicted to be a TI.⁷⁰ The DFT band structure of the bulk phase has a finite bandgap, whereas the surface states display metallic behavior and form a Dirac cone at the Γ point (Figure 6a).

Recently, Simpson et al. as well as Tominaga and co-workers^{71,72} designed a new storage scheme that exploits fast and reversible transitions occurring in crystalline $\text{Ge}_2\text{Sb}_2\text{Te}_5$ superlattices. This concept, dubbed interfacial phase-change memory (iPCM), could lead to significantly lower power consumption.⁷¹ Although the switching mechanism is not fully understood, it is believed to be due to transitions between different stacking sequences (Figure 6b). The contrast in electrical resistance could originate

from the different topological properties of the relevant phases.^{70,72,73} For this reason, iPCMs are also referred to as topological-switching random-access memories. Therefore, a DFT-based understanding of the topological properties of GST compounds is not only theoretically interesting, but also of practical value.

The properties of PCMs can be enhanced and expanded by doping with small amounts of adatoms: The exploration and design of suitable dopants offer intriguing possibilities for experimental–theoretical collaboration. For example, Prasai et al.,⁷⁴ Skelton et al.,⁷⁵ and Zhu et al.⁷⁶ showed that additions of silver, bismuth, and titanium, respectively, can improve the crystallization kinetics of GST and Sb_2Te_3 at high temperatures. It was reported by Song et al.⁷⁷ that Fe-doped GST is ferromagnetic in both phases, which, however, display pronounced contrast in saturation magnetization (~30%). Hence, doping with transition-metal atoms might lead to magnetic switching in PCMs. Design rules on dopant selection

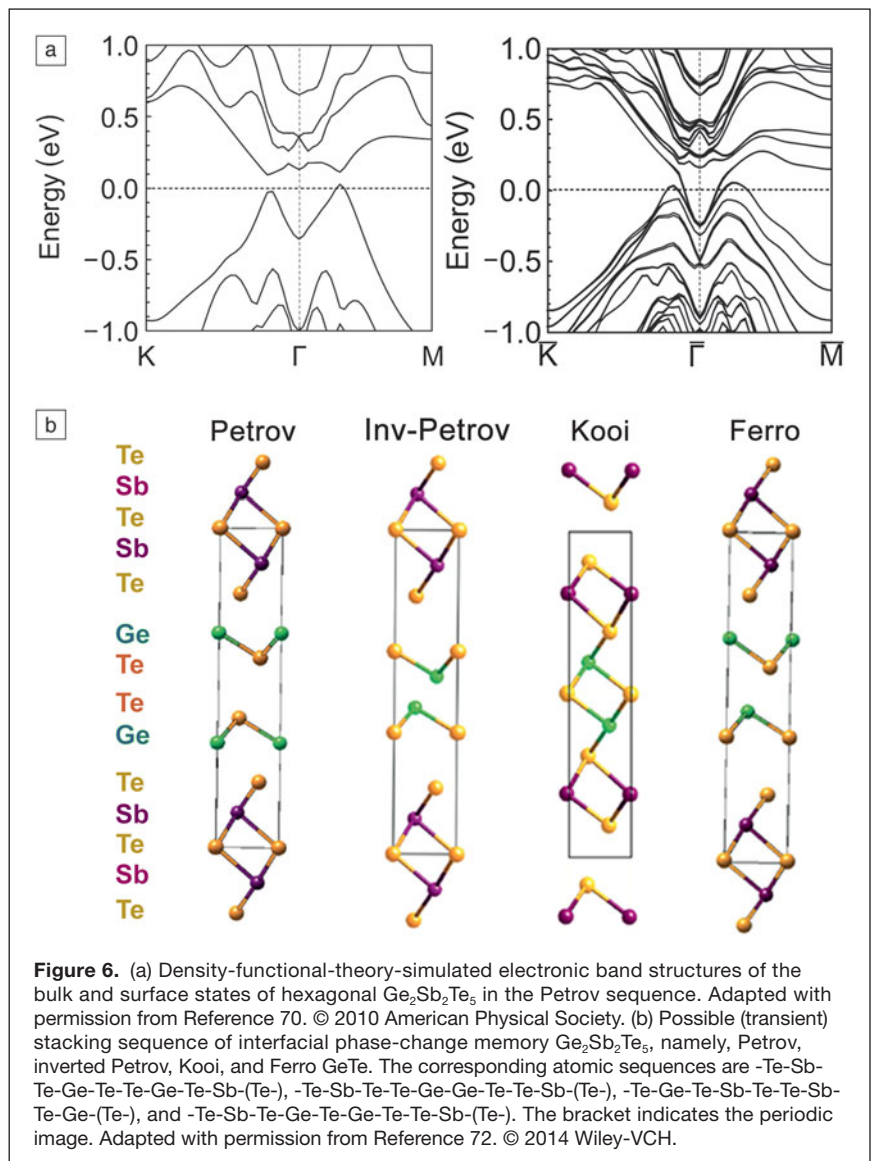


Figure 6. (a) Density-functional-theory-simulated electronic band structures of the bulk and surface states of hexagonal $\text{Ge}_2\text{Sb}_2\text{Te}_5$ in the Petrov sequence. Adapted with permission from Reference 70. © 2010 American Physical Society. (b) Possible (transient) stacking sequence of interfacial phase-change memory $\text{Ge}_2\text{Sb}_2\text{Te}_5$, namely, Petrov, inverted Petrov, Kooi, and Ferro GeTe . The corresponding atomic sequences are $-\text{Te}-\text{Sb}-\text{Te}-\text{Ge}-\text{Te}-\text{Te}-\text{Ge}-\text{Te}-\text{Sb}-(\text{Te}-)$, $-\text{Te}-\text{Sb}-\text{Te}-\text{Te}-\text{Ge}-\text{Te}-\text{Te}-\text{Sb}-(\text{Te}-)$, $-\text{Te}-\text{Ge}-\text{Te}-\text{Sb}-\text{Te}-\text{Te}-\text{Ge}-\text{Te}-(\text{Te}-)$, and $-\text{Te}-\text{Sb}-\text{Te}-\text{Ge}-\text{Te}-\text{Ge}-\text{Te}-\text{Te}-\text{Sb}-(\text{Te}-)$. The bracket indicates the periodic image. Adapted with permission from Reference 72. © 2014 Wiley-VCH.

for magnetic PCMs were recently proposed based on DFT simulations.^{78–80}

What might other materials-science fields learn from these examples?

Before closing, we note that the experience gained and lessons learned from employing DFT calculations in the thriving field of PCMs and memories, through both successful and failed attempts, could be instructive to the materials science community at large. The specific examples discussed in this article are illustrative of the power of DFT-based approaches: systematic simulations to construct design rules to find better-performance compounds; large-scale DFT simulations to uncover new physics, such as disorder-induced phenomena and crystallization kinetics of complex systems (ternary, quaternary, etc.); enhanced sampling techniques for rare events such as nucleation; DFT-trained neural-network potentials to reduce computational costs; quenching-time issues in the kinetic properties of fragile systems; electronic-level understanding of the nature of chemical bonding in highly disordered amorphous materials; the use of chemical substitution methods to describe relaxation mechanisms in the amorphous state; detection of unusual electronic properties of topological phases and the switching processes between them; tailoring of materials performance through doping; and manipulation of magnetic properties with phase-change cycles. These DFT simulations revealed atomistic mechanisms on the electronic structure level, and as such, supplement laboratory experiments in explaining the observed properties. Whenever possible, the DFT predictions should be checked against experimental findings to bridge the gap between a “real-life” device and a quantum-mechanical approximant to it.

We believe that other materials-science fields would benefit from similar tactics. For instance, extending our analysis of the crystallization of PCM glass discussed earlier, large-scale DFMD simulations might unravel the atomistics of crystallization kinetics (propagation speed of the crystal front) in elemental metallic glasses,⁸¹ which have so far remained unexplainable using all current models and MD simulations. State-of-the-art DFT calculations are also instrumental in uncovering the unprecedented impact of defects on the electronic structure of two-dimensional materials.^{82,83} *Ab initio* design rules can be developed in many fields, including engineering materials such as steels.⁸⁴ Local bonding analysis methods should shed light on other complex amorphous materials.⁸⁵ Incidentally, in this endeavor, PRAM-equipped supercomputers could very well turn out to be the enabling vehicle that makes these developments feasible in the near future.

Acknowledgments

W.Z., V.L.D., R.D., R.M., and M.W. gratefully acknowledge funding from Deutsche Forschungsgemeinschaft (DFG) within SFB 917 (“Nanoswitches”). W.Z. and M.W. acknowledge ERC Advanced Grant *Disorder Control*. W.Z. gratefully thanks the Young Talent Support Plan of Xi’an Jiaotong University.

E.M. acknowledges support from US DoE-BES-DMSE, DE-FG02-13ER46056.

References

1. M. Wuttig, N. Yamada, *Nat. Mater.* **6**, 824 (2007).
2. T. Siegrist, P. Merkelbach, M. Wuttig, *Annu. Rev. Condens. Matter Phys.* **3**, 215 (2012).
3. S. Raoux, F. Xiong, M. Wuttig, E. Pop, *MRS Bull.* **39**, 703 (2014).
4. S.R. Elliott, *Int. J. Appl. Glass Sci.* **6**, 15 (2015).
5. M.H. Lankhorst, B.W. Ketelaars, R.A. Wolters, *Nat. Mater.* **4**, 347 (2005).
6. R.M. Martin, *Electronic Structure: Basic Theory and Practical Methods* (Cambridge University Press, Cambridge, UK, 2004).
7. D. Marx, J. Hutter, *Ab Initio Molecular Dynamics: Basic Theory and Advanced Methods* (Cambridge University Press, Cambridge, UK, 2009).
8. V.L. Deringer, R. Dronskowski, M. Wuttig, *Adv. Funct. Mater.*, published online June 10, 2015, <http://dx.doi.org/10.1002/adfm.201500826>.
9. K. Shportko, S. Kremers, M. Woda, D. Lencer, J. Robertson, M. Wuttig, *Nat. Mater.* **7**, 653 (2008).
10. D. Lencer, M. Salinga, B. Grabowski, T. Hickel, J. Neugebauer, M. Wuttig, *Nat. Mater.* **7**, 972 (2008).
11. B. Huang, J. Robertson, *Phys. Rev. B* **81**, 081204(R) (2010).
12. S. Caravati, M. Bernasconi, M. Parrinello, *J. Phys. Condens. Matter* **22**, 315801 (2010).
13. N. Yamada, *MRS Bull.* **21**, 48 (1996).
14. T. Matsunaga, N. Yamada, *Phys. Rev. B* **69**, 104111 (2004).
15. M. Wuttig, D. Lusebrink, D. Wamwangi, W. Welnic, M. Gillessen, R. Dronskowski, *Nat. Mater.* **6**, 122 (2007).
16. R. Dronskowski, P.E. Blöchl, *J. Phys. Chem.* **97**, 8617 (1993).
17. U.V. Waghmare, N.A. Spaldin, H.C. Kandpal, R. Seshadri, *Phys. Rev. B* **67**, 125111 (2003).
18. R.P. Stoffel, V.L. Deringer, R.E. Simon, R.P. Hermann, R. Dronskowski, *J. Phys. Condens. Matter* **27**, 085402 (2015).
19. T. Siegrist, P. Jost, H. Volker, M. Woda, P. Merkelbach, C. Schlockermann, M. Wuttig, *Nat. Mater.* **10**, 202 (2011).
20. A. Edwards, A. Pineda, P. Schultz, M. Martin, A. Thompson, H. Hjalmarsen, C. Umrigar, *Phys. Rev. B* **73**, 045210 (2006).
21. S. Caravati, M. Bernasconi, T.D. Kühne, M. Krack, M. Parrinello, *J. Phys. Condens. Matter* **21**, 255501 (2009).
22. H. Volker, P. Jost, M. Wuttig, *Adv. Funct. Mater.*, published online June 10, 2015, <http://dx.doi.org/10.1002/adfm.201500830>.
23. W. Zhang, A. Thiess, P. Zalden, R. Zeller, P.H. Dederichs, J.Y. Raty, M. Wuttig, S. Blügel, R. Mazzarello, *Nat. Mater.* **11**, 952 (2012).
24. S. Caravati, M. Bernasconi, T.D. Kühne, M. Krack, M. Parrinello, *Appl. Phys. Lett.* **91**, 171906 (2007).
25. J. Akola, R. Jones, *Phys. Rev. B* **76**, 235201 (2007).
26. J. Hegedüs, S.R. Elliott, *Nat. Mater.* **7**, 399 (2008).
27. J. Akola, R. Jones, *Phys. Rev. B* **79**, 134118 (2009).
28. M. Xu, Y.Q. Cheng, L. Wang, H.W. Sheng, Y. Meng, W.G. Yang, X.D. Han, E. Ma, *Proc. Natl. Acad. Sci. U.S.A.* **109**, E1055 (2012).
29. A.V. Kolobov, P. Fons, A.I. Frenkel, A.L. Ankudinov, J. Tominaga, T. Uruga, *Nat. Mater.* **3**, 703 (2004).
30. M. Xu, Y. Cheng, H. Sheng, E. Ma, *Phys. Rev. Lett.* **103**, 195502 (2009).
31. R. Mazzarello, S. Caravati, S. Angioletti-Uberti, M. Bernasconi, M. Parrinello, *Phys. Rev. Lett.* **104**, 085503 (2010).
32. M. Micoulaut, J.Y. Raty, C. Otjacques, C. Bichara, *Phys. Rev. B* **81**, 174206 (2010).
33. E. Cho, J. Im, C. Park, W.J. Son, D.H. Kim, H. Horii, J. Ihm, S. Han, *J. Phys. Condens. Matter* **22**, 205504 (2010).
34. B. Cai, D.A. Drabold, S.R. Elliott, *Appl. Phys. Lett.* **97**, 191908 (2010).
35. A.V. Kolobov, M. Krbal, P. Fons, J. Tominaga, T. Uruga, *Nat. Chem.* **3**, 311 (2011).
36. X.-B. Li, X.Q. Liu, X. Liu, D. Han, Z. Zhang, X.D. Han, H.-B. Sun, S.B. Zhang, *Phys. Rev. Lett.* **107**, 015501 (2011).
37. M. Micoulaut, A. Kachmar, T. Charpentier, *Phys. Status Solidi B* **249**, 1890 (2012).
38. M. Krbal, A.V. Kolobov, P. Fons, K.V. Mitrofanov, Y. Tamenori, J. Hegedüs, S.R. Elliott, J. Tominaga, *Appl. Phys. Lett.* **102**, 111904 (2013).
39. K.V. Mitrofanov, A.V. Kolobov, P. Fons, X. Wang, J. Tominaga, Y. Tamenori, T. Uruga, N. Ciocchini, D. Ielmini, *J. Appl. Phys.* **115**, 173501 (2014).
40. V.L. Deringer, W. Zhang, M. Lumeij, S. Maintz, M. Wuttig, R. Mazzarello, R. Dronskowski, *Angew. Chem. Int. Ed.* **53**, 10817 (2014).
41. V.L. Deringer, A.L. Tchougréeff, R. Dronskowski, *J. Phys. Chem. A* **115**, 5461 (2011).
42. S. Maintz, V.L. Deringer, A.L. Tchougréeff, R. Dronskowski, *J. Comput. Chem.* **34**, 2557 (2013).
43. J.-Y. Raty, W. Zhang, J. Luckas, C. Chen, C. Bichara, R. Mazzarello, M. Wuttig, *Nat. Commun.* **6**, 7467 (2015).

44. H.-S. P. Wong, S. Raoux, S.B. Kim, J. Liang, J.P. Reifenberg, B. Rajendran, M. Asheghi, K.E. Goodson, *Proc. IEEE* **98**, 2201 (2010).
45. D. Ielmini, A.L. Lacaita, D. Mantegazza, *IEEE Trans. Electron Devices* **54**, 308 (2007).
46. P. Fantini, S. Brazzelli, E. Cazzini, A. Mani, *Appl. Phys. Lett.* **100**, 013505 (2012).
47. D. Krebs, T. Bachmann, P. Jonnalagadda, L. Dellmann, S. Raoux, *New J. Phys.* **16**, 043015 (2014).
48. J. Kalikka, J. Akola, R.O. Jones, *Phys. Rev. B* **90**, 184109 (2014).
49. W. Zhang, I. Ronneberger, P. Zalden, M. Xu, M. Salinga, M. Wuttig, R. Mazzarello, *Sci. Rep.* **4**, 6529 (2014).
50. E.R. Meinders, A.V. Mijiritskii, L. van Pieterse, M. Wuttig, *Optical Data Storage: Phase-Change Media and Recording* (Springer, Dordrecht, The Netherlands, 2006).
51. T.H. Lee, S.R. Elliott, *Phys. Rev. Lett.* **107**, 145702 (2011).
52. J. Kalikka, J. Akola, J. Larrucea, R.O. Jones, *Phys. Rev. B* **86**, 144113 (2012).
53. I. Ronneberger, W. Zhang, H. Eshet, R. Mazzarello, *Adv. Funct. Mater.*, published online May 5, 2015, <http://dx.doi.org/10.1002/adfm.201500849>.
54. A. Laio, M. Parrinello, *Proc. Natl. Acad. Sci. U.S.A.* **99**, 12562 (2002).
55. A. Sebastian, M. Le Gallo, D. Krebs, *Nat. Commun.* **5**, 4314 (2014).
56. J. Orava, A.L. Greer, B. Gholipour, D.W. Hewak, C.E. Smith, *Nat. Mater.* **11**, 279 (2012).
57. R. Jeyasingh, S.W. Fong, J. Lee, Z. Li, K.W. Chang, D. Mantegazza, M. Asheghi, K.E. Goodson, H.S. Wong, *Nano Lett.* **14**, 3419 (2014).
58. Z. Sun, J. Zhou, R. Ahuja, *Phys. Rev. Lett.* **96**, 055507 (2006).
59. J. Da Silva, A. Walsh, H. Lee, *Phys. Rev. B* **78**, 224111 (2008).
60. C. Pauly, M. Liebmann, A. Giussani, J. Kellner, S. Just, J. Sánchez-Barriga, E. Rienks, O. Rader, R. Calarco, G. Bihlmayer, M. Morgenstern, *Appl. Phys. Lett.* **103**, 243109 (2013).
61. D. Loke, T.H. Lee, W.J. Wang, L.P. Shi, R. Zhao, Y.C. Yeo, T.C. Chong, S.R. Elliott, *Science* **336**, 1566 (2012).
62. G.C. Sosso, G. Miceli, S. Caravati, J. Behler, M. Bernasconi, *Phys. Rev. B* **85**, 174103 (2012).
63. G. Sosso, G. Miceli, S. Caravati, F. Giberti, J. Behler, M. Bernasconi, *J. Phys. Chem. Lett.* **4**, 4241 (2013).
64. G. Sosso, J. Colombo, J. Behler, E. Del Gado, M. Bernasconi, *J. Phys. Chem. B* **118**, 13621 (2014).
65. T. Matsunaga, J. Akola, S. Kohara, T. Honma, K. Kobayashi, E. Ikenaga, R.O. Jones, N. Yamada, M. Takata, R. Kojima, *Nat. Mater.* **10**, 129 (2011).
66. M. Salinga, E. Carria, A. Kaldenbach, M. Bornhofft, J. Benke, J. Mayer, M. Wuttig, *Nat. Commun.* **4**, 2371 (2013).
67. P.G. Debenedetti, F.H. Stillinger, *Nature* **410**, 259 (2001).
68. H. Zhang, C.-X. Liu, X.-L. Qi, X. Dai, Z. Fang, S.-C. Zhang, *Nat. Phys.* **5**, 438 (2009).
69. M.Z. Hasan, C.L. Kane, *Rev. Mod. Phys.* **82**, 3045 (2010).
70. J. Kim, J. Kim, S.-H. Jhi, *Phys. Rev. B* **82**, 201312(R) (2010).
71. R.E. Simpson, P. Fons, A.V. Kolobov, T. Fukaya, M. Krbal, T. Yagi, J. Tominaga, *Nat. Nanotechnol.* **6**, 501 (2011).
72. J. Tominaga, A.V. Kolobov, P. Fons, T. Nakano, S. Murakami, *Adv. Mater. Interfaces* **1**, 1300027 (2014).
73. B. Sa, J. Zhou, Z. Sun, J. Tominaga, R. Ahuja, *Phys. Rev. Lett.* **109**, 096802 (2012).
74. B. Prasai, M.E. Kordesch, D.A. Drabold, G. Chen, *Phys. Status Solidi B* **250**, 1785 (2013).
75. J.M. Skelton, A.R. Pallipurath, T.-H. Lee, S.R. Elliott, *Adv. Funct. Mater.* **24**, 7291 (2014).
76. M. Zhu, M. Xia, F. Rao, X. Li, L. Wu, X. Ji, S. Lv, Z. Song, S. Feng, H. Sun, S. Zhang, *Nat. Commun.* **5**, 4086 (2014).
77. W.-D. Song, L.-P. Shi, X.-S. Miao, C.-T. Chong, *Adv. Mater.* **20**, 2394 (2008).
78. D. Ding, K. Bai, W.D. Song, L.P. Shi, R. Zhao, R. Ji, M. Sullivan, P. Wu, *Phys. Rev. B* **84**, 214416 (2011).
79. W. Zhang, I. Ronneberger, Y. Li, R. Mazzarello, *Adv. Mater.* **24**, 4387 (2012).
80. J.M. Skelton, S.R. Elliott, *J. Phys. Condens. Matter* **25**, 205801 (2013).
81. A.L. Greer, *Nat. Mater.* **14**, 542 (2015).
82. K.S. Novoselov, V.I. Fal'ko, L. Colombo, P.R. Gellert, M.G. Schwab, K. Kim, *Nature* **490**, 192 (2012).
83. Q.H. Wang, K. Kalantar-Zadeh, A. Kis, J.N. Coleman, M.S. Strano, *Nat. Nanotechnol.* **7**, 699 (2012).
84. T. Hickey, A. Dick, B. Grabowski, F. Körmann, J. Neugebauer, *Steel Res. Int.* **80**, 4 (2010).
85. K. Nomura, H. Ohta, A. Takagi, T. Kamiya, M. Hirano, H. Hosono, *Nature* **432**, 488 (2004). □



Wei Zhang is an associate professor and a distinguished research fellow of materials science and engineering at Xi'an Jiaotong University, Xi'an, China, where he is supported by the university's Young Talent Support Plan. He received bachelor's and master's degrees in physics from Zhejiang University, Hangzhou China, and a PhD degree from RWTH Aachen University, Aachen, Germany, under the guidance of Riccardo Mazzarello and Matthias Wuttig. His current research interests include electronic and memory materials, first-principles materials design, and materials behavior at the nanoscale. Zhang can be reached by email at wzhang0@mail.xjtu.edu.cn.



Volker L. Deringer is a postdoctoral researcher at RWTH Aachen University, Aachen, Germany, as of this writing, and will start a postdoc at the University of Cambridge, UK, in October 2015. He obtained his diploma in 2010 and doctorate in 2014, both under the guidance of Richard Dronskowski at RWTH. He has been awarded fellowships from the German National Academic Foundation and, recently, from the Alexander von Humboldt Foundation. His research interests concern the chemical-bonding nature of solids, including surfaces, defects, and amorphous materials. Deringer can be reached by email at volker.deringer@ac.rwth-aachen.de.



Richard Dronskowski is a full professor of chemistry at RWTH Aachen University, Aachen, Germany, where he holds the Chair of Solid-State and Quantum Chemistry. He obtained his doctorate under the guidance of Arndt Simon at Stuttgart University, Stuttgart, Germany, and worked with Roald Hoffmann at Cornell University (Ithaca, N.Y.) as a visiting scientist. After receiving his habilitation in 1995, he joined RWTH, where he was elected Distinguished Professor in 2014. His research interests comprise synthetic solid-state chemistry (carbodiimides, guanidines, and nitrides), neutron diffraction, and condensed-matter theory (electronic structure, chemical bonding, and thermochemistry). Dronskowski can be reached by email at drons@HAL9000.ac.rwth-aachen.de.



Riccardo Mazzarello is a junior professor in theoretical nanoelectronics at RWTH Aachen University, Aachen, Germany, where he has been since December 2009. He is a computational physicist working in the field of condensed-matter physics, mesoscopic physics, and materials science. His main research interests include phase-change materials, graphene nanostructures, and self-assembled monolayers of organic molecules deposited on metallic substrates, which he investigates using *ab initio* methods based on density functional theory. Mazzarello can be reached by email at mazzarello@physik.rwth-aachen.de.



Evan Ma is a full professor of materials science and engineering at Johns Hopkins University (JHU), Baltimore, Md. He also holds an adjunct professorship at Xi'an Jiaotong University, Xi'an, China. He did his undergraduate and graduate studies at Tsinghua University, Beijing, China, and California Institute of Technology (Pasadena, Calif.) and postdoctoral work at Massachusetts Institute of Technology (Cambridge, Mass.). Prior to JHU, he was an assistant and associate professor at Louisiana State University. He has published ~300 papers and presented ~110 invited talks at international conferences. His current research interests include metallic glasses,

chalcogenide phase-change alloys, nanostructured metals, plasticity mechanisms, and *in situ* TEM of small-volume materials. He is an elected Fellow of ASM, APS, and MRS. Ma can be reached by email at ema@jhu.edu.



Matthias Wuttig is a full professor of physics at RWTH Aachen University, Aachen, Germany, where his research focus is the understanding and tailoring of materials with unique optical and electrical properties. He received a diploma in physics from the University of Cologne, Köln, Germany, and a PhD degree from Forschungszentrum Jülich/RWTH Aachen. He is speaker on the Strategy Board of RWTH Aachen and has served as Dean of the faculty of science, mathematics, and computer sciences. He is the coordinator of the Collaborative Research Centre "Nanoswitches." His awards include an ERC Advanced Grant in 2013. Wuttig can be reached by email at wuttig@physik.rwth-aachen.de.

iMatSci

Spring 2016

Innovation in Materials Science

Held during the 2016 MRS Spring Meeting & Exhibit, iMatSci—Innovation in Materials Science will provide materials-based startups with a platform to demonstrate the practical applications of their technologies, while connecting these innovators to potential sources of venture capital. An international pool of startups will be judged by professional technology innovators and will compete for cash prizes.

Spanning parts of two days, iMatSci will start with an Entrepreneurial Skills Workshop on Tuesday afternoon. Wednesday's Innovator Demonstration Program will kick off with a keynote address on "Transformational Innovation" followed by a panel on venture investing.

Demonstration Schedule

Tuesday, March 29

Entrepreneurial Skills Workshop

Wednesday, March 30

Innovator Demonstrations/Venture Panel

Phoenix Convention Center



2016 **MRS**[®]
SPRING MEETING & EXHIBIT
March 28–April 1, 2016 | Phoenix, Arizona

Submit an iMatSci Innovator Demonstration Application!
Application Deadline—December 15

www.mrs.org/spring-2016-imatsci

iMatSci is part of the new MRS Innovation ConneXions—a collection of programs and resources to help connect people and ideas ... provide access to innovation-related expertise ... and initiate the process of interaction and collaboration. For more information about MRS Innovation ConneXions and other innovation-related events, resources and opportunities, visit www.mrs.org/innovation-connexions.

MRS Innovation ConneXions
Connecting People and Ideas